

Entangled photon holes-boosted quantum teleportation of Schrödinger-cat states

Kaushik P. Seshadreesan,^{1,*} Jonathan P. Dowling,^{1,2} and Girish S. Agarwal³

¹Hearne Institute for Theoretical Physics and Department of Physics and Astronomy,
Louisiana State University, Baton Rouge, LA 70803, USA

²Beijing Computational Science Research Center, Beijing, 100084, China

³Department of Physics, Oklahoma State University, Stillwater, OK 74078, USA

(Dated: December 3, 2024)

We study the teleportation of non-Gaussian, non-classical Schrödinger-cat states of light. We use the experimentally realized cat states produced by subtracting a photon from the single-mode squeezed vacuum state of light. We introduce a new resource for teleportation in the form of two-mode squeezed vacuum light embedded with entangled photon holes. We characterize the resource by showing how the holes appear in the quadrature distribution of the state. We discuss two figures of merit for the teleportation process, a) the fidelity, and b) the maximum negativity of the Wigner function at the output. We show that the addition of entangled photon holes to two-mode squeezed vacuum light lowers the requirements on the amount of squeezing necessary to achieve any given fidelity of teleportation, or to achieve negative values of the Wigner function at the output.

© 2024 Optical Society of America

OCIS codes: 270.0270, 270.6570, 270.5585

1. Introduction

Quantum mechanics allows for the transport of the unknown state of a quantum system, *i.e.*, its information content, without having to transport the “baggage” of its mass. Bennett *et al.* invented a first-of-the-kind protocol, which demonstrated such a transport for qubit states with the help of a) a shared entangled resource between the sender and the receiver in the form of a Bell state, b) Bell-basis measurements, and c) classical communication¹. Since the transport involved destroying the state at the sender (Alice’s location) and recreating it at the receiver (Bob’s), albeit after some time lapse, they called it “teleportation”. Later, Vaidman, Braunstein and Kimble (VBK) devised a continuous-variable (CV) version of the protocol, which used the two-mode squeezed vacuum state of the quantized electromagnetic field (TMSV) for shared entanglement and homodyne detection for performing measurements analogous to Bell-basis measurements^{2,3}.

Quantum teleportation forms an important building block for quantum information processing. In quantum communication, sequential teleportation can be used to transport quantum states over large distances^{4,5}. In quantum computation, several teleportation-based schemes that are capable of implementing two-qubit (or interaction) gates near-deterministically (and in a fault tolerant manner) have been proposed in both the discrete and continuous quantum variable cases^{6,7}; examples of

teleportation-based coupling gates include the controlled sign-flip CZ gate in linear optical quantum computation⁸, and the QND interaction gate in CV quantum computation^{9,10}. In some hybrid quantum computation schemes, wherein the physical qubits used for computation “talk” to each other via CV channels, CV teleportation facilitates the communication¹¹.

CV quantum information processing¹² primarily revolves around the use of Gaussian states such as the coherent state, and Gaussian operations such as the passive linear optical transformations of the beam splitter and the phase shifter, the displacement operation, as well as the squeezing operation which involves quadratic optical nonlinearities. While Gaussian states and operations alone suffice for some basic quantum information protocols, such as quantum-key distribution based on coherent states, the more advanced protocols, *e.g.*, those for universal quantum computation, entanglement-distillation-based quantum communication, etc., require the use of at least third-order optical nonlinearities¹³. Non-Gaussian CV states, which result from such higher-order optical nonlinear interactions, *e.g.*, the Schrödinger-cat state

$$|\Psi_{\text{cat}}\rangle = N^{-1} (|+\alpha_0\rangle + e^{i\theta} |-\alpha_0\rangle), \quad (1)$$

where $N = \sqrt{2(1 + e^{-2|\alpha_0|^2} \cos \theta)}$ and $|\pm \alpha_0\rangle$ are coherent states, when used in conjunction with linear optics, have been shown to fulfill such requirements¹⁴. The ability to teleport non-Gaussian states such as the cat state thus is critical in order to accomplish advanced quantum information processing tasks.

Several theoretical works have examined the teleportation of the cat state $|\Psi_{\text{cat}}\rangle$ of Eq. (1) using a va-

*Electronic address: ksesha1@lsu.edu

riety of resources^{15–19}. However, experimentally, the state $|\Psi_{\text{cat}}\rangle$ for radiation fields has not been produced. The standard procedure adopted by several experimental groups^{20–23} has been to subtract a photon from a single-mode squeezed vacuum state to produce a state like the state $|\Psi_{\text{cat}}\rangle$ for $\theta = \pi^{24}$. In this work, we thus consider the heralded production of such a cat state, and study its teleportation. The cat state heralded in the above fashion is defined by

$$|\Phi_{\text{cat}}\rangle = \frac{1}{\sinh r} \hat{a} \hat{S}(\xi) |0\rangle, \quad \xi = \rho e^{i\varphi}, \quad (2)$$

where $\hat{S}(\xi) = \exp((\xi \hat{a}^{\dagger 2} - \xi^* \hat{a}^2)/2)^{25}$ is the single-mode squeezing operator acting on the mode \hat{a} .

The teleportation of Gaussian states, such as the coherent state, has been demonstrated in many experiments since 1998 with high fidelities^{26–29}. However, the first-ever teleportation of a non-Gaussian state was carried out rather recently²³. Using the standard VBK protocol for CV teleportation with TMSV as the entangled resource, Lee *et al.* teleported a cat state $|\Phi_{\text{cat}}\rangle$ of Eq. (2) of $75 \pm 0.5\%$ input state fidelity with respect to the cat state $|\Psi_{\text{cat}}\rangle$ of coherent amplitude $|\alpha|^2 \approx 1$ and $\theta = \pi$, achieving an output fidelity of $45 \pm 1\%$ with respect to the same cat state^{23,30,31}. Apart from fidelity, another important figure of merit for teleportation, in the case of non-Gaussian input states, is the maximum negativity of the output Wigner function relative to the input. Lee *et al.* observed that, in their experiment, the negativity of the input Wigner function remained preserved at the output to a degree that was in good agreement with the prediction based on a model for non-unity gain teleportation given by Mista *et al.*³².

Since TMSV provides the shared entanglement for the standard protocol of CV teleportation, obviously both the fidelity and the maximum negativity of the Wigner function at the output are ultimately limited by the squeezing resource. In the limit of infinite squeezing, since TMSV tends to become the EPR state³³ with perfect correlations, the fidelity of teleportation also approaches unity. Despite leaps in technological advancement, the state-of-the-art vacuum squeezing for TMSV, however, remains about 10 dB^{34,35}. Hence, techniques that improve the performance of teleportation without demanding higher magnitudes of squeezing are vital commodities in quantum information. In this regard, for any given amount of squeezing, TMSV which is made non-Gaussian via photon addition or subtraction³⁶, has been known to contain more entanglement than TMSV^{37,38}. Hence, non-Gaussian entangled states should be better suited for teleportation^{15–19}.

In an independent development Franson, in 2006, showed that correlated photon absences generated via two-photon absorption from a coherent laser beam incident on an absorption medium, could be used to violate Bell's inequalities in a manner akin to entangled photons themselves³⁹. He called them entangled photon holes (EPH). The existence of such photon holes was

further established by Pittman and Franson through a proof-of-principle experiment based on the mixing of coherent laser light with squeezed vacuum light from the output of a parametric down-conversion (PDC) source on a 50-50 beam splitter⁴⁰. When the two inputs are mixed out of phase, the probability amplitudes (two of them—one for each input) corresponding to two photons incident in the same input mode getting split at the 50:50 beam splitter, perfectly cancel each other, leading to the generation of a correlated absence of single photons, or, an EPH pair, in the output modes. Afek *et al.* generalized the experiment by also varying the ratio of intensities of the coherent and PDC output, and they observed higher-order correlated photon-holes⁴¹. In this work, we show that a conditional measurement based on simultaneous subtraction of a photon from each of the two modes of TMSV light results in the introduction of a structure similar to that of an EPH pair discussed by Franson originally using atomic absorbers. We thus establish a link between the two different lines of research. We then use the EPH-containing TMSV resource for the teleportation of the experimentally realized cat state $|\Phi_{\text{cat}}\rangle$.

The paper is organized as follows. In section 2, we discuss the generation of EPH-embedded TMSV, and demonstrate the existence of an EPH pair in the state using its photon number and quadrature distributions. We then show that the entanglement content of EPH-embedded TMSV is higher than TMSV. In section 3, we describe quantum teleportation based on EPH-embedded TMSV, and present our results on the fidelity and the maximum negativity of the Wigner function at the output for input cat states of Eq. (2) generated from the single-mode squeezed vacuum state via photon subtraction. In section 4, we highlight the enhanced fidelity that EPH-embedded-TMSV also offers in the teleportation of two of the most commonly used Gaussian states, namely the coherent state and the single-mode squeezed vacuum state. We conclude with a summary in section 5.

2. Entangled photon holes-embedded two-mode squeezed vacuum light

A. Generation

Consider the scheme shown in Fig. 1. Parametric down-conversion generates a two-mode squeezed-vacuum state $|\xi\rangle$, given by

$$|\xi\rangle = \hat{S}(\xi) |0, 0\rangle, \quad \xi = r e^{i\phi}, \quad (3)$$

where $\hat{S}(\xi) = \exp(\xi \hat{a}^{\dagger} \hat{b}^{\dagger} - \xi^* \hat{a} \hat{b})^{25}$, and \hat{a} and \hat{b} are the mode operators of the two-mode output field. Highly transmissive beam splitters, one placed in each of the two modes of TMSV, feed single-photon detectors (SPD-1, 2). When the SPDs register a coincidence detection,

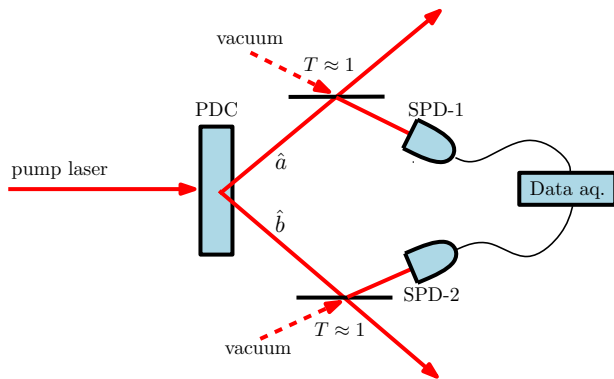


Fig. 1. (Color online) A conditional measurement scheme, wherein a photon is subtracted from each of the two modes of TMSV. PDC stands for parametric down-conversion, and the SPDs are single photon detectors.

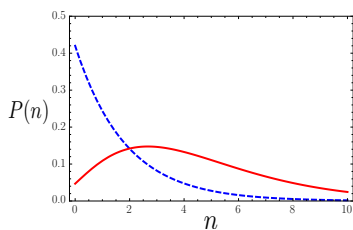


Fig. 2. (Color online) The photon number distributions for TMSV (dashed, blue) and two-photon subtracted TMSV (solid, red) for the squeezing parameter $r = 1$. $P(n)$ corresponds to the probability of finding n photons in each of the two modes simultaneously.

the state heralded by the scheme can be written as

$$\begin{aligned}
 |\xi\rangle_{\text{EPH}} &\propto \hat{a}\hat{b}\hat{S}(\xi)|0\rangle|0\rangle \\
 &= \frac{1}{\sqrt{1+\tanh^2 r}} \hat{S}(\xi) (|0, 0\rangle + e^{i\phi} \tanh r |1, 1\rangle) \\
 &= \frac{1}{\cosh^3 r \sqrt{1+\tanh^2 r}} \sum_{n=0}^{\infty} e^{in\phi} (\tanh r)^n (n+1) |n, n\rangle,
 \end{aligned} \tag{4}$$

where the state has been suitably normalized. Here we note that the conditional measurement scheme for the generation of the cat state $|\Phi_{\text{cat}}\rangle$, whose teleportation we discuss later in this paper, is very similar to the scheme of Fig. 1 (the difference being the former involves only a single mode PDC output and a single SPD^{23,24,31}).

Figure 2 shows plots of the photon number distributions of TMSV and the state heralded in the scheme of Fig. 1, $|\xi\rangle_{\text{EPH}}$, for the squeezing parameter $r = 1$. We find that the latter has a higher weighting for large photon numbers than TMSV, as was also observed by Cochrane *et al.* in Ref.¹⁶. Consequently, the probability of measuring single photon coincidences in the two modes of the state $|\xi\rangle_{\text{EPH}}$ is substantially reduced compared to that of TMSV. Particularly, this effect is found to grow larger as the value of the squeezing parameter r is increased. The ratio $P_{\text{EPH}}(1)/P_{\text{TMSV}}(1)$ for the squeezing parameter $r = 1$ (shown in Fig. 2) is about 0.3, while its value dwindles to $\approx 6 \times 10^{-8}$ when $r = 5$. This decrease in probability of single photon coincidences with the state $|\xi\rangle_{\text{EPH}}$ is similar to the creation of EPH pairs in Franson's work³⁹.

B. Quadrature distribution

We now discuss the quadrature distribution of the state $|\xi\rangle_{\text{EPH}}$, and show how EPH appear in the distribution in a remarkable way. For quadrature operators $\hat{x}_a, \hat{y}_a, \hat{x}_b,$ and \hat{y}_b defined in terms of the mode operators $\hat{a}, \hat{a}^\dagger, \hat{b},$ and \hat{b}^\dagger as

$$\begin{aligned}
 \hat{x}_a &= \frac{1}{\sqrt{2}} (\hat{a} + \hat{a}^\dagger), & \hat{y}_a &= \frac{1}{\sqrt{2}i} (\hat{a} - \hat{a}^\dagger), \\
 \hat{x}_b &= \frac{1}{\sqrt{2}} (\hat{b} + \hat{b}^\dagger), & \hat{y}_b &= \frac{1}{\sqrt{2}i} (\hat{b} - \hat{b}^\dagger),
 \end{aligned} \tag{5}$$

the quadrature distribution of TMSV, which is well known⁴², and that of two-photon subtracted TMSV, which can be calculated using Eq. (4), are given by

$$\begin{aligned}
 \psi_\xi(x_a, x_b) &= \frac{1}{\sqrt{(1-\eta^2)\pi \cosh^2 r}} \exp\left[\frac{2x_a x_b \eta - (x_a^2 + x_b^2)\eta^2}{1-\eta^2} - \frac{1}{2}(x_a^2 + x_b^2)\right], \\
 \psi_{\text{EPH}}(x_a, x_b) &= N^{-1} \eta (1 + \eta \frac{\partial}{\partial \eta}) \psi_\xi(x_a, x_b), \quad \left(\eta = e^{i\phi} \tanh r, \quad N = \sinh r \cosh r \sqrt{1 + \tanh^2 r}\right),
 \end{aligned} \tag{6}$$

respectively, where x_a, x_b are the eigenvalues values of the corresponding quadrature operators. The states $|\xi\rangle$ and $|\psi_{\text{EPH}}\rangle$, both, are clearly entangled. It is advantageous to work with a rotated set of coordinates x_1 and

x_2 , defined as

$$x_1 = \frac{x_a + x_b}{\sqrt{2}}, \quad x_2 = \frac{x_a - x_b}{\sqrt{2}}. \tag{7}$$

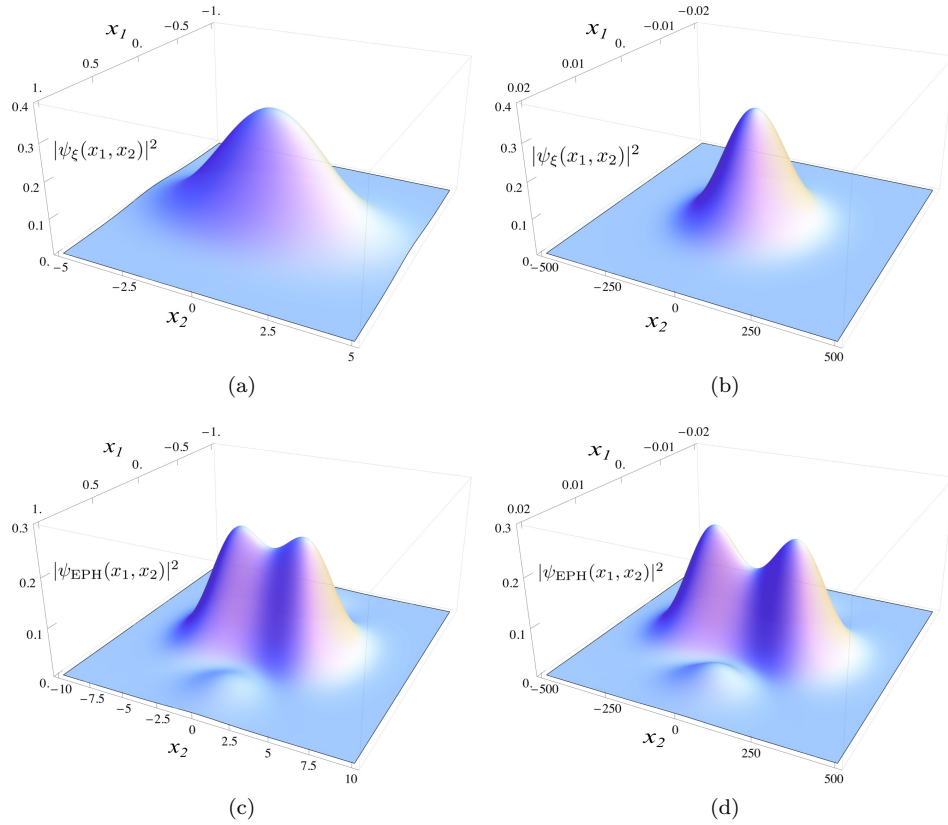


Fig. 3. (Color online) (a) and (b) The intensity $|\psi_\xi(x_1, x_2)|^2$ as a function of x_1 and x_2 , when the squeezing parameters are chosen to be $r = 1$, $\phi = \pi$, and $r = 5$, $\phi = \pi$, respectively. (c) and (d) The intensity $|\psi_{\text{EPH}}(x_1, x_2)|^2$ as a function of x_1 and x_2 when the squeezing parameters are chosen to be $r = 1$, $\phi = \pi$, and $r = 5$, $\phi = \pi$, respectively.

In terms of x_1 and x_2 , the state $|\xi\rangle$ has quite a transparent structure in its quadrature distribution

$$\psi_\xi(x_1, x_2) = \frac{1}{\sqrt{(1-\eta^2)\pi \cosh^2 r}} e^{-\frac{1}{2}\left(\frac{1-\eta}{1+\eta}\right)x_1^2} e^{-\frac{1}{2}\left(\frac{1+\eta}{1-\eta}\right)x_2^2}. \quad (8)$$

When $\phi = \pi$, as is well known, Eq. (8) has the EPR form with a narrow peak at $x_1 = 0$

$$\psi_\xi(x_1, x_2) = \frac{1}{\sqrt{\pi}} e^{-x_1^2/(2e^{-2r})} e^{-x_2^2/(2e^{2r})}. \quad (9)$$

Fig. 3 shows the intensities $|\psi_\xi(x_1, x_2)|^2$ and $|\psi_{\text{EPH}}(x_1, x_2)|^2$ plotted as functions of x_1 and x_2 for values of the squeezing parameter $r = 1$ and $r = 5$. We find that the plot of $|\psi_{\text{EPH}}(x_1, x_2)|^2$ shows a dip at $x_2 = 0$. Since $x_2 \propto x_a - x_b$, the dip signifies a decrease in the probability of finding photons at the same values of position quadratures in the two modes for the state $|\xi\rangle_{\text{EPH}}$. Between Figs. 3(c) and 3(d), we find that the dip at $x_2 = 0$ is even more pronounced in the latter, which corresponds to the larger value of squeezing parameter r .

The dip observed in the quadrature distributions of Figs. 3(c) and 3(d), along with the decrease in the photon number probabilities for small photon numbers shown in Fig. 2, indicate a decrease in the probability of coincidence detection of single photons in the two modes of

the state $|\xi\rangle_{\text{EPH}}$. This is similar in fashion to Franson's observation of a decrease in the probability of two-photon coincidence detection in a classical field after the field has passed through a two-photon absorbing medium. Thus, in line with Franson's argument, we argue that the dip is a consequence of the existence of a pair of EPH in the state $|\xi\rangle_{\text{EPH}}$.

C. The logarithmic-negativity parameter

We now discuss the entanglement content of the “EPH-embedded TMSV” $|\xi\rangle_{\text{EPH}}$. An appropriate entanglement measure in the case of CV states is the so-called logarithmic-negativity parameter^{43,44}, which is defined as

$$\varepsilon = \log_2(1 + 2\mathcal{N}), \quad (10)$$

where \mathcal{N} is the absolute value of the sum of all negative eigenvalues associated with the partial transpose of the density operator. By proceeding along the lines of Eqs. (20)–(23) of Ref.³⁸, the log-negativity parameters of EPH-embedded TMSV and TMSV are calculated, and found to be

$$\begin{aligned} \varepsilon_\xi &= \log_2(e^{2r}), \\ \varepsilon_{\text{EPH}} &= \log_2(e^{4r}/\cosh 2r). \end{aligned} \quad (11)$$

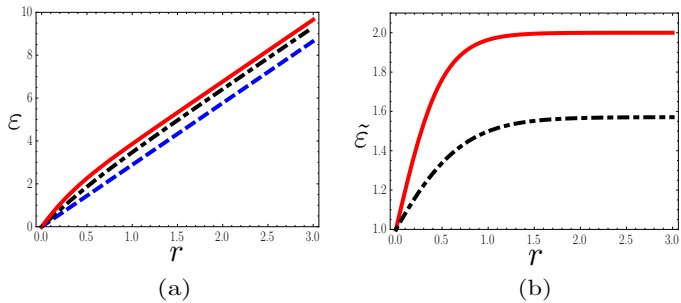


Fig. 4. (Color online) (a) The log-negativity parameter ε for TMSV (dashed, blue), photon-added (dot-dashed, black), and EPH-embedded (solid, red) TMSV as a function of the squeezing parameter r . (b) The ratio $\tilde{\varepsilon}$ for photon-added (dot-dashed, black) and EPH-embedded (solid, red) TMSV as a function of the squeezing parameter r .

(See Appendix A for the derivation.) Figure 4 (a) shows a plot of the log-negativity parameters of EPH-embedded TMSV, single-photon-added TMSV⁴⁵ and TMSV, plotted as a function of the squeezing parameter r . As one can see, in terms of log-negativity, EPH-embedded TMSV is more entangled than the single-photon-added TMSV, which is in turn more entangled than TMSV. The ratio $\tilde{\varepsilon} = 2^\varepsilon/2^{\varepsilon_\varepsilon}$ magnifies the difference between the entanglement content of the photon-added or EPH-embedded TMSV with respect to TMSV. Fig. 4 (b) shows a plot of $\tilde{\varepsilon}$ for both the photon-added and EPH-embedded TMSV, as a function of the squeezing parameter r .

3. Quantum teleportation of Schrödinger-cat states using entangled-photon-holes-embedded two-mode squeezed vacuum light

Having shown that the EPH-embedded TMSV is more entangled than TMSV, we now describe CV quantum teleportation based on the former, and examine its performance in the teleportation of non-Gaussian, non-classical Schrödinger-cat states in comparison to teleportation based on the latter (the standard protocol).

To begin with, let us briefly describe CV teleportation, as introduced by VBK (see Fig. 5). Alice, who wants to transport a single-mode input state to Bob, prearranges the sharing of an entangled resource with him. She mixes the single-mode input state (in mode \hat{a}') with mode \hat{a} of the entangled resource on a 50:50 beam splitter. She then performs a homodyne measurement on the beam-splitter-output modes and classically communicates the result $\mu = q + ip$ to Bob. Assuming balanced homodyning, the real and imaginary parts of μ satisfy

$$\frac{1}{\sqrt{2}} (\hat{x}_{a'} - \hat{x}_a) |q\rangle = q|q\rangle, \quad \frac{1}{\sqrt{2}} (\hat{y}_{a'} + \hat{y}_a) |p\rangle = p|p\rangle, \quad (12)$$

where \hat{x}_a , \hat{y}_a , $\hat{x}_{a'}$ and $\hat{y}_{a'}$ are the canonical operators probed by the homodyne measurement, which are related to the beam-splitter-input mode operators \hat{a} , \hat{a}'

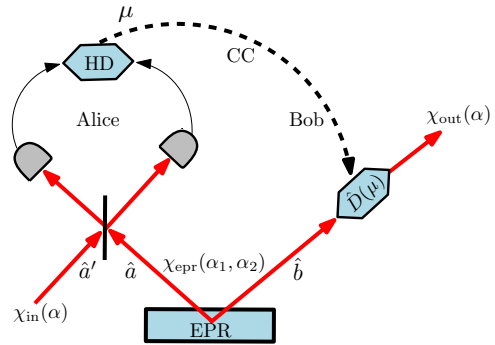


Fig. 5. (Color online) A schematic of the VBK protocol for CV teleportation. HD, CC stand for homodyne detection and classical communication, respectively. EPR refers to the entangled resource shared between Alice and Bob. In this work, it is either TMSV or EPH-embedded TMSV.

in a manner similar to the relation given in Eq. (5). As a final step, Bob performs a displacement operation $\hat{D}(\mu) = \exp(\mu\hat{b}^\dagger - \mu^*\hat{b})$ on the mode \hat{b} of the entangled resource, which results in the recovery of the teleported state.

Mathematically, the above protocol can be described via one of many alternative approaches¹². We adopt an approach based on the use of characteristic functions. The Weyl-ordered characteristic function of a single-mode pure state $|\psi\rangle$ is given by $\chi(\alpha) = \langle\psi|\hat{D}(\alpha)|\psi\rangle$, where $\hat{D}(\alpha)$ is the displacement operator. The Wigner function is related to the Weyl-ordered characteristic function via a Fourier transform, as

$$W(\beta) = \frac{1}{\pi^2} \int d^2\alpha \chi(\alpha) e^{\beta\alpha^* - \beta^*\alpha}. \quad (13)$$

Marian and Marian⁴⁶ showed that, assuming ideal measurements and the case that Alice performs balanced homodyne detection, the Weyl-ordered characteristic function of the teleportation output (χ_{out}) can be written in terms of those of the input (χ_{in}) and the entangled resource (χ_{EPR}) as

$$\chi_{out}(\alpha) = \chi_{in}(\alpha)\chi_{EPR}(\alpha^*, \alpha). \quad (14)$$

We now calculate two figures of merit for the teleportation of non-Gaussian, nonclassical cat state $|\Phi_{cat}\rangle$ of Eq. (2)—the fidelity and the maximum negativity of the Wigner function at the output—for both TMSV and EPH-embedded TMSV entangled resources. The characteristic function of the input cat state $\chi_\Phi(\alpha) = \langle\Phi|\hat{D}(\alpha)|\Phi\rangle$ is given by

$$\chi_\Phi(\alpha; \rho, \varphi) = (1 - |\tilde{\alpha}|^2) e^{-|\tilde{\alpha}|^2/2}, \quad \tilde{\alpha} = \alpha \cosh \rho - \exp(i\varphi)\alpha^* \sinh \rho, \quad (15)$$

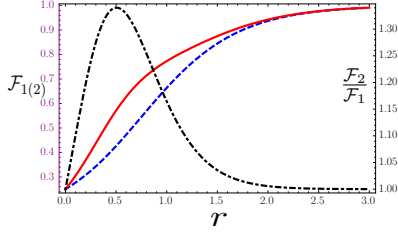


Fig. 6. (Color online) (Left hand side vertical scale) The teleportation fidelity $\mathcal{F}_{1(2)}$ for the optimal cat state $|\Phi_{\text{cat}}\rangle$ corresponding to the state $|\Psi_{\text{cat}}\rangle$ with $|\alpha_0| = 1$ and $\theta = \pi$, when teleported using TMSV \mathcal{F}_1 (dashed, blue), and when teleported using EPH-embedded TMSV \mathcal{F}_2 (solid, red), plotted as a function of the squeezing parameter r . (Right hand side vertical scale) The ratio of the two fidelities $\mathcal{F}_2/\mathcal{F}_1$ (dot-dashed, black), plotted as a function of the squeezing parameter r .

and those associated with the entangled resources, TMSV ($\chi_\xi = \langle \xi | \hat{D}(\alpha) \otimes \hat{D}(\beta) | \xi \rangle$) and EPH-embedded TMSV ($\chi_{\text{EPH}} = \langle \xi_{\text{EPH}} | \hat{D}(\alpha) \otimes \hat{D}(\beta) | \xi_{\text{EPH}} \rangle$), are given by

$$\begin{aligned} \chi_\xi(\alpha_1, \alpha_2) &= e^{-1/2(|\xi_1|^2 + |\xi_2|^2)}, \\ \chi_{\text{EPH}}(\alpha_1, \alpha_2) &= \chi_\xi(\alpha_1, \alpha_2) \\ &\times \frac{1 - 2 \tanh r \text{Re}[e^{-i\phi} \xi_1 \xi_2] + \tanh^2 r (1 - |\xi_1|^2)(1 - |\xi_2|^2)}{1 + \tanh^2 r}, \end{aligned} \quad (16)$$

respectively, where

$$\xi_k = \alpha_k \cosh r + \alpha_l^* e^{i\phi} \sinh r, \quad (k, l = 1, 2; k \neq l). \quad (17)$$

A. Fidelity of teleportation

The fidelity of teleportation $|\langle \psi_{\text{in}} | \psi_{\text{out}} \rangle|^2$, when written in terms of characteristic functions reads

$$\begin{aligned} \mathcal{F} &= \frac{1}{\pi} \int d^2\alpha \chi_{\text{in}}(\alpha) \chi_{\text{out}}(-\alpha), \\ &= \frac{1}{\pi} \int d^2\alpha \chi_{\text{in}}(\alpha) \chi_{\text{in}}(-\alpha) \chi_{\text{EPR}}(-\alpha^*, -\alpha). \end{aligned} \quad (18)$$

Using Eqs. (14)–(17) in Eq. (18), the expressions for the teleportation fidelity for the state $|\Phi_{\text{cat}}\rangle$, when teleported optimally⁴⁷ using TMSV (\mathcal{F}_1) and EPH-embedded TMSV (\mathcal{F}_2), are found to be

$$\begin{aligned} \mathcal{F}_1(\rho, \varphi, \gamma) &= \frac{2 + 4\gamma \cosh 2\rho + (1 + 3 \cosh 4\rho)\gamma^2 + 4\gamma^3 \cosh 2\rho + 2\gamma^4}{2(1 + 2\gamma \cosh 2\rho + \gamma^2)^{5/2}}, \\ \mathcal{F}_2(\rho, \varphi, \gamma) &= \hat{\Gamma} \mathcal{F}_1(\rho, \varphi, \gamma), \\ \hat{\Gamma} &= \left[1 + \frac{\gamma^2(1+\gamma)^2}{2(1+\gamma^2)} \left\{ \left(\frac{1-\gamma}{1+\gamma} \right)^2 \frac{\partial^2}{\partial \gamma^2} - 4 \frac{1-\gamma}{(1+\gamma)^2} \frac{\partial}{\partial \gamma} \right\} \right], \end{aligned} \quad (19)$$

respectively, where $\gamma = e^{-2r}$. (See Appendix B for the derivation of \mathcal{F}_2 .)

We now focus on the state $|\Phi_{\text{cat}}\rangle$ corresponding to $|\Psi_{\text{cat}}\rangle$ of coherent amplitude $|\alpha_0| = 1$ and $\theta = \pi$. The optimal choice $\rho = 0.313$ in Eq. (2) provides an input-state fidelity of 99.7%^{48,49}. Fig. 6 shows a plot of the

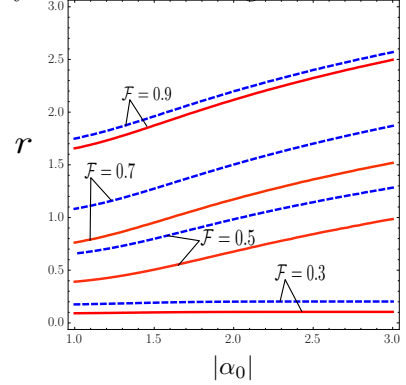


Fig. 7. (Color online) A contour plot of the teleportation fidelity \mathcal{F} for the optimal cat state $|\Phi_{\text{cat}}\rangle$ corresponding to the state $|\Psi_{\text{cat}}\rangle$ of different coherent amplitudes $|\alpha_0|$ and $\theta = \pi$, for different values of squeezing parameter r of the entangled resources, namely, TMSV (dashed, blue), EPH-embedded TMSV (solid, red).

two teleportation fidelities, and their ratio for the teleportation of the above cat state as a function of the squeezing parameter of the entangled resource r . We see that EPH-embedded TMSV offers substantially enhanced fidelity over TMSV for small values of the squeezing parameter r ($0 < r < 2$). Figure 7 shows a contour plot of the optimal fidelity of teleportation for the cat state $|\Phi_{\text{cat}}\rangle$ corresponding to different magnitudes $|\alpha_0|$ of $|\Psi_{\text{cat}}\rangle$ with $\theta = \pi$, as a function of the coherent amplitude $|\alpha_0|$ and the squeezing parameter of the entangled resource r . (The squeezing parameter ρ for the different input states $|\Phi_{\text{cat}}\rangle$ is chosen such that the input-state fidelity is maximized.) The plot elucidates the persistence of the squeezing benefit in using EPH-embedded TMSV in place of TMSV for cat states of Eq. (1) with increasing values of coherent amplitude $|\alpha_0|$.

B. Maximum negativity of the Wigner function at the output

The Wigner function of the state $|\Phi_{\text{cat}}\rangle$ of Eq. (2) is given by

$$W(\alpha; \rho, \varphi) = \frac{2}{\pi} \left(4|\tilde{\alpha}|^2 - 1 \right) e^{-2|\tilde{\alpha}|^2}, \quad (20)$$

where $\tilde{\alpha} = \alpha \cosh \rho - \exp(i\varphi) \alpha^* \sinh \rho$. Based on Eqs. (13)–(17), the Wigner functions at the output of the teleportation process, when teleported optimally⁴⁷ using TMSV (W_1) and EPH-embedded TMSV (W_2), are found to be

$$\begin{aligned}
W_1(\alpha; \rho, \varphi, \gamma) &= \frac{2}{\pi(1+4\gamma \cosh 2\rho+4\gamma^2)^{5/2}} \exp\left(\frac{-2}{1+4\gamma \cosh 2\rho+4\gamma^2}(2\gamma|\alpha|^2 + |\tilde{\alpha}|^2)\right) \\
&\times \left[(4|\tilde{\alpha}|^2 - 1) + 4\left(4|\alpha|^2 - \cosh 2\rho\right)\gamma + 16\left(3|\tilde{\alpha}|^2 - 2|\alpha|^2 \cosh 2\rho\right)\gamma^2 + 16\gamma^3 \cosh 2\rho + 16\gamma^4 \right], \\
W_2(\alpha; \rho, \varphi, \gamma) &= \hat{\Gamma}W_1(\alpha; \rho, \varphi, \gamma),
\end{aligned} \tag{21}$$

respectively, where $\hat{\Gamma}$ is the differential operator given in Eq. (19). Figures 8 and 9, show plots of the Wigner function of the optimal cat state $|\Phi_{\text{cat}}\rangle$ corresponding to the state $|\Psi_{\text{cat}}\rangle$ with $|\alpha_0| = 1$ and $\theta = \pi$, at the input and output of the teleportation process, respectively. The Wigner functions in Fig. 9(a) and (b) correspond to the output states of the teleportation process with TMSV and EPH-embedded TMSV as the entangled resources, respectively, at a value of the squeezing parameter (of the entangled resource) $r = 0.5$. The chosen value of r corresponds to that point at which the ratio of fidelities $\mathcal{F}_2/\mathcal{F}_1$ is maximum in Fig. 6. We find that the Wigner function teleported using EPH-embedded TMSV achieves a lower negative value (0.2) than the one teleported using TMSV (0.05).

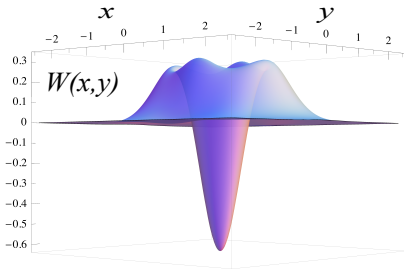


Fig. 8. (Color online) Wigner function of the optimal cat state $|\Phi_{\text{cat}}\rangle$ corresponding to the state $|\Psi_{\text{cat}}\rangle$ with $|\alpha_0| = 1$ and $\theta = \pi$.

As is obvious from Fig. 8, the Wigner function of the optimal cat state $|\Phi_{\text{cat}}\rangle$ corresponding to the state $|\Psi_{\text{cat}}\rangle$ with $|\alpha_0| = 1$ reaches its maximum negative value at the phase-space origin. Figure 10 shows a plot of $W(0)$ of the Wigner function of this state at the output of the teleportation process, as a function of the squeezing parameter of the entangled resource r . The plot illustrates the fact that the threshold value of the squeezing parameter r , above which the value of $W(0)$ at the output of the teleportation process becomes negative, is smaller when EPH-embedded TMSV is used ($r = 0.2$), as compared to the value when TMSV is used ($r = 0.35$). Also, the former becomes more negative than the latter in the range of $0 < r < 2$.

In this investigation, we have not considered the deterioration of the fidelity due to finite efficiency of the detectors. However, these can be examined by follow-

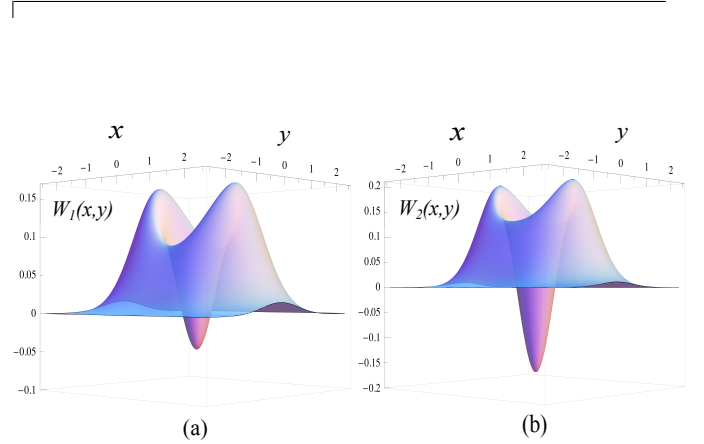


Fig. 9. (Color online) Wigner function of the optimal cat state $|\Phi_{\text{cat}}\rangle$ corresponding to the state $|\Psi_{\text{cat}}\rangle$ with $|\alpha_0| = 1$ and $\theta = \pi$, at the output of the teleportation process, when teleported using (a) TMSV (left), (b) EPH-embedded TMSV (right). The squeezing parameter r is chosen to be 0.5. The Wigner function teleported using EPH-embedded TMSV achieves a much lower negative value (0.2) than the value achieved by using TMSV (0.05).

ing the standard procedure, *e.g.*, as used by Olivares *et al.*^{17,18}.

4. Entangled-photon-hole-booster teleportation of Gaussian states

For the sake of completeness, in this section, we present EPH-embedded TMSV-based teleportation for two of the most commonly used Gaussian states, namely the coherent state and the single-mode squeezed vacuum state¹⁹. Characteristic functions of the coherent and single-mode squeezed vacuum states are given by

$$\begin{aligned}
\chi_{\text{coh}}(\alpha; \alpha_0) &= \exp\left(\frac{-1}{2}|\alpha|^2 + 2i\text{Im}[\alpha\alpha_0^*]\right), \\
\chi_{\text{sqv}}(\alpha; \rho, \varphi) &= \exp\left(\frac{-1}{2}|\alpha^* \cosh \rho + e^{-i\varphi}\alpha \sinh \rho|^2\right),
\end{aligned} \tag{22}$$

respectively. The optimal teleportation fidelities for the above states when teleported using TMSV and EPH-

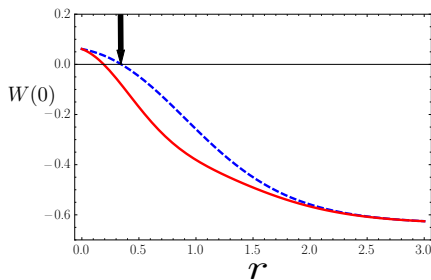


Fig. 10. (Color online) Wigner function at the phase-space origin for the optimal cat state $|\Phi_{\text{cat}}\rangle$ corresponding to the state $|\Psi_{\text{cat}}\rangle$ with $|\alpha_0| = 1$ and $\theta = \pi$, when teleported using TMSV (dashed, blue) and EPH-embedded TMSV (solid, red). Negative values of the Wigner function of the teleported state are achieved at a smaller value of the squeezing parameter r for EPH-embedded TMSV ($r = 0.2$, against $r = 0.35$ for TMSV, as indicated by the arrow).

embedded TMSV, calculated based on Eq. (18), are tabulated in Table 1.

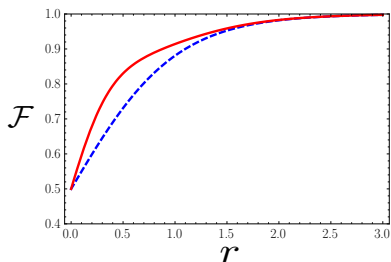


Fig. 11. (Color online) A plot of the teleportation fidelity \mathcal{F} for coherent states, as a function of the squeezing parameter r of the entangled resources, namely, TMSV (dashed, blue), EPH-embedded TMSV (bold, red).

For coherent states, the enhancement to the fidelity of teleportation due to EPH-embedded TMSV is independent of the amplitude of the state, as can be seen in Fig. 11. Figure 12 presents a contour plot for the fidelity of teleportation of the single mode squeezed vacuum state as a function of the squeezing parameters r and ρ . The contours illustrate the fact that at any value of the squeezing parameter ρ of the single-mode squeezed state, EPH-TMSV achieves the same fidelity of teleportation as TMSV while requiring a smaller amount of the squeezing resource. Thus, EPH-embedded TMSV offers enhanced teleportation not only for non-Gaussian states, but also Gaussian states.

5. Summary

In summary, we showed how the resource based on EPH can be used to teleport nonclassical Schrödinger cat states with high fidelity. In particular, we showed that the EPH-embedded TMSV achieves a higher maximum

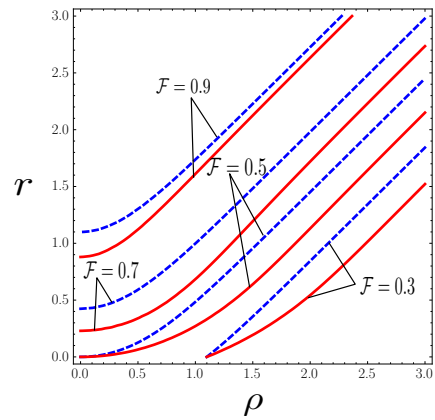


Fig. 12. (Color online) A contour plot of the teleportation fidelity \mathcal{F} for single mode squeezed vacuum states $|\xi_0\rangle$ of different values of parameter $\rho = |\xi_0|$, for different values of squeezing parameter r of the entangled resources, namely, TMSV (dashed, blue), EPH-embedded TMSV (bold, red).

negativity of the teleported Wigner function than TMSV at any given amount of utilization of the squeezing-resource. The EPH-embedded resource, thus, enables one to recover the nonclassical properties of the teleported state better. We established the nature of EPH, which we create by photon subtraction. We showed how the holes appear in the quadrature distribution at the point where the two mode squeezed vacuum has a peak. Our results illustrate the usefulness of EPH in continuous-variable quantum information processing.

6. Acknowledgments

KPS thanks the Oklahoma State University for the hospitality, while this work was initiated. JPD would like to acknowledge the support from the AFOSR and the NSF.

References

1. C. H. Bennett, G. Brassard, C. Crépeau, R. Jozsa, A. Peres, and W. K. Wootters, “Teleporting an unknown quantum state via dual classical and einstein-podolsky-rosen channels,” *Phys. Rev. Lett.* **70**, 1895–1899 (1993).
2. L. Vaidman, “Teleportation of quantum states,” *Phys. Rev. A* **49**, 1473–1476 (1994).
3. S. L. Braunstein and H. J. Kimble, “Teleportation of continuous quantum variables,” *Phys. Rev. Lett.* **80**, 869–872 (1998).
4. H.-J. Briegel, W. Dür, J. I. Cirac, and P. Zoller, “Quantum repeaters: The role of imperfect local operations in quantum communication,” *Phys. Rev. Lett.* **81**, 5932–5935 (1998).
5. L.-M. Duan, M. D. Lukin, J. I. Cirac, and P. Zoller, “Long-distance quantum communication with atomic ensembles and linear optics,” *Nature* **414**, 413–418 (2001).

State	\mathcal{F}_1	\mathcal{F}_2
$ \alpha_0\rangle$	$\frac{1}{1+\gamma}$	$\frac{1+2\gamma+5\gamma^2}{(1+\gamma)^3(1+\gamma^2)}$
$ \xi_0\rangle$	$\frac{1}{\sqrt{1+2\gamma \cosh 2\rho+\gamma^2}}$	$\frac{1}{4(1+\gamma)^2} \frac{1}{(\sqrt{1+2\gamma \cosh 2\rho+\gamma^2})^5} \times [c_4\gamma^4 + c_3\gamma^3 + c_2\gamma^2 + c_1 + c_0]$

Table 1. Teleportation fidelities for a coherent state $|\alpha_0\rangle$ and a single-mode squeezed vacuum state $|\xi_0\rangle$, teleported using TMSV (\mathcal{F}_1) and EPH-embedded TMSV (\mathcal{F}_2), where $\gamma = e^{-2r}$, $c_4 = 3 \cosh 4\rho + 8 \cosh 2\rho + 9$, $c_3 = 2 \cosh 4\rho + 32 \cosh 2\rho + 14$, $c_2 = 11 \cosh 4\rho + 8 \cosh 2\rho + 21$, $c_1 = 16 \cosh 2\rho$ and $c_0 = 4$.

6. D. Gottesman and I. L. Chuang, “Demonstrating the viability of universal quantum computation using teleportation and single-qubit operations,” *Nature* **402**, 390–393 (1999).
7. S. D. Bartlett and W. J. Munro, “Quantum teleportation of optical quantum gates,” *Phys. Rev. Lett.* **90**, 117901 (2003).
8. E. Knill, R. Laflamme, and G. J. Milburn, “A scheme for efficient quantum computation with linear optics,” *Nature* **409**, 46–52 (2001).
9. R. Filip, P. Marek, and U. L. Andersen, “Measurement-induced continuous-variable quantum interactions,” *Phys. Rev. A* **71**, 042308 (2005).
10. J.-i. Yoshikawa, Y. Miwa, A. Huck, U. L. Andersen, P. van Loock, and A. Furusawa, “Demonstration of a quantum nondemolition sum gate,” *Phys. Rev. Lett.* **101**, 250501 (2008).
11. P. van Loock, W. J. Munro, K. Nemoto, T. P. Spiller, T. D. Ladd, S. L. Braunstein, and G. J. Milburn, “Hybrid quantum computation in quantum optics,” *Phys. Rev. A* **78**, 022303 (2008).
12. S. L. Braunstein and P. van Loock, “Quantum information with continuous variables,” *Rev. Mod. Phys.* **77**, 513–577 (2005).
13. S. Lloyd and S. L. Braunstein, “Quantum computation over continuous variables,” *Phys. Rev. Lett.* **82**, 1784–1787 (1999).
14. T. C. Ralph, A. Gilchrist, G. J. Milburn, W. J. Munro, and S. Glancy, “Quantum computation with optical coherent states,” *Phys. Rev. A* **68**, 042319 (2003).
15. T. Opatrný, G. Kurizki, and D.-G. Welsch, “Improvement on teleportation of continuous variables by photon subtraction via conditional measurement,” *Phys. Rev. A* **61**, 032302 (2000).
16. P. T. Cochrane, T. C. Ralph, and G. J. Milburn, “Teleportation improvement by conditional measurements on the two-mode squeezed vacuum,” *Phys. Rev. A* **65**, 062306 (2002).
17. S. Olivares, M. G. A. Paris, and R. Bonifacio, “Teleportation improvement by inconclusive photon subtraction,” *Phys. Rev. A* **67**, 032314 (2003).
18. S. Olivares and M. G. A. Paris, “Enhancement of nonlocality in phase space,” *Phys. Rev. A* **70**, 032112 (2004).
19. F. Dell’Anno, S. De Siena, L. Albano, and F. Illuminati, “Continuous-variable quantum teleportation with non-gaussian resources,” *Phys. Rev. A* **76**, 022301 (2007).
20. A. Ourjoumtsev, R. Tualle-Brouiri, J. Laurat, and P. Grangier, “Generating optical schrödinger kittens for quantum information processing,” *Science* **312**, 83–86 (2006).
21. T. Gerrits, S. Glancy, T. S. Clement, B. Calkins, A. E. Lita, A. J. Miller, A. L. Migdall, S. W. Nam, R. P. Mirin, and E. Knill, “Generation of optical coherent-state superpositions by number-resolved photon subtraction from the squeezed vacuum,” *Phys. Rev. A* **82**, 031802 (2010).
22. N. Namekata, Y. Takahashi, G. Fujii, D. Fukuda, S. Kurimura, and S. Inoue, “Non-gaussian operation based on photon subtraction using a photon-number-resolving detector at a telecommunications wavelength,” *Nat Photon* **4**, 655 (2010).
23. N. Lee, H. Benichi, Y. Takeno, S. Takeda, J. Webb, E. Huntington, and A. Furusawa, “Teleportation of nonclassical wave packets of light,” *Science* **332**, 330–333 (2011).
24. M. Dakna, T. Anhut, T. Opatrný, L. Knöll, and D.-G. Welsch, “Generating schrödinger-cat-like states by means of conditional measurements on a beam splitter,” *Phys. Rev. A* **55**, 3184–3194 (1997).
25. C. C. Gerry and P. L. Knight, *Introductory Quantum Optics*, Cambridge University Press (2005).
26. Fidelity of teleportation is the overlap of the input state with the output state.
27. A. Furusawa, J. L. Sørensen, S. L. Braunstein, C. A. Fuchs, H. J. Kimble, and E. S. Polzik, “Unconditional quantum teleportation,” *Science* **282**, 706–709 (1998).
28. W. P. Bowen, N. Treps, B. C. Buchler, R. Schnabel, T. C. Ralph, H.-A. Bachor, T. Symul, and P. K. Lam, “Experimental investigation of continuous-variable quantum teleportation,” *Phys. Rev. A* **67**, 032302 (2003).
29. H. Yonezawa, T. Aoki, and A. Furusawa, “Non-gaussian operation based on photon subtraction using a photon-number-resolving detector at a telecommunications wavelength,” *Nature* **431**, 430 (2004).
30. Here, by input and output fidelities, we mean the overlap of the input and output states with the cat state $|\Psi_{\text{cat}}\rangle$ of Eq. (1), respectively.
31. P. Grangier, “Make it quantum and continuous,” *Science* **332**, 313–314 (2011).
32. L. Mista, R. Filip, and A. Furusawa, “Continuous-variable teleportation of a negative wigner function,” *Phys. Rev. A* **82**, 012322 (2010).

33. A. Einstein, B. Podolsky, and N. Rosen, “Can quantum-mechanical description of physical reality be considered complete?” *Phys. Rev.* **47**, 777–780 (1935).
34. T. Eberle, V. Händchen, and R. Schnabel, “Stable control of 10 db two-mode squeezed vacuum states of light,” *Opt. Express* **21**, 11546–11553 (2013).
35. H. Vahlbruch, M. Mehmet, S. Chelkowski, B. Hage, A. Franzen, N. Lastzka, S. Goßler, K. Danzmann, and R. Schnabel, “Observation of squeezed light with 10-db quantum-noise reduction,” *Phys. Rev. Lett.* **100**, 033602 (2008).
36. G. S. Agarwal and K. Tara, “Nonclassical properties of states generated by the excitations on a coherent state,” *Phys. Rev. A* **43**, 492–497 (1991).
37. A. Kitagawa, M. Takeoka, M. Sasaki, and A. Chefles, “Entanglement evaluation of non-gaussian states generated by photon subtraction from squeezed states,” *Phys. Rev. A* **73**, 042310 (2006).
38. G. S. Agarwal, “Engineering non-gaussian entangled states with vortices by photon subtraction,” *New Journal of Physics* **13**, 073008 (2011).
39. J. D. Franson, “Entangled photon holes,” *Phys. Rev. Lett.* **96**, 090402 (2006).
40. T. B. Pittman and J. D. Franson, “Generation of entangled photon holes using quantum interference,” *Phys. Rev. A* **74**, 041801 (2006).
41. I. Afek, O. Ambar, and Y. Silberberg, “Correlated multiphoton holes: Absence of multiphoton coincidence events,” *Phys. Rev. Lett.* **105**, 093603 (2010).
42. G. S. Agarwal, *Quantum Optics*, Cambridge University Press (2012).
43. G. Vidal and R. F. Werner, “Computable measure of entanglement,” *Phys. Rev. A* **65**, 032314 (2002).
44. M. B. Plenio, “Logarithmic negativity: A full entanglement monotone that is not convex,” *Phys. Rev. Lett.* **95**, 090503 (2005).
45. The single-photon-added TMSV can be found in Eqs. (8) and (9) of Ref.³⁸.
46. P. Marian and T. A. Marian, “Continuous-variable teleportation in the characteristic-function description,” *Phys. Rev. A* **74**, 042306 (2006).
47. Optimality is achieved when in Eq. (17) the squeezing angle ϕ of the entangled resource is set to π .
48. H. Jeong, A. P. Lund, and T. C. Ralph, “Production of superpositions of coherent states in traveling optical fields with inefficient photon detection,” *Phys. Rev. A* **72**, 013801 (2005).
49. The phase φ is set to be 0, in order to fix a phase reference.

Appendix A

The logarithmic negativity ε of a state can be calculated using the absolute sum of the negative eigenvalues $\mathcal{N} = |\sum_i \lambda_i|$, $\lambda_i < 0$ of the partial transpose of its density operator ρ^{PT} , as $\varepsilon = \log(1 + \mathcal{N})$. The partial transpose

ρ^{PT} corresponding to the state of Eq. (4) is given by

$$\rho^{\text{PT}} = \sum_{n,m=0}^{\infty} c_n c_m e^{i(n-m)\phi} |n, m\rangle \langle m, n|,$$

$$c_n = \frac{\tanh^n r}{\cosh^3 r \sqrt{1 + \tanh^2 r}} (n+1). \quad (\text{A1})$$

Clearly, the diagonal terms in Eq. (A1) are all positive. The off-diagonal terms ($n \neq m$) in Eq. (A1) have the form

$$|n, m\rangle \langle m, n| e^{i(n-m)\phi} + |m, n\rangle \langle n, m| e^{i(m-n)\phi}, \quad (\text{A2})$$

which can be diagonalized as

$$\begin{aligned} & \left(\frac{e^{in\phi} |n, m\rangle + e^{im\phi} |m, n\rangle}{\sqrt{2}} \right) \left(\frac{e^{-in\phi} \langle n, m| + e^{-im\phi} \langle m, n|}{\sqrt{2}} \right) \\ & - \left(\frac{e^{in\phi} |n, m\rangle - e^{im\phi} |m, n\rangle}{\sqrt{2}} \right) \left(\frac{e^{-in\phi} \langle n, m| - e^{-im\phi} \langle m, n|}{\sqrt{2}} \right). \end{aligned} \quad (\text{A3})$$

Thus, all the negative eigenvalues are $-c_n c_m$, and hence the logarithmic negativity parameter becomes

$$\begin{aligned} \varepsilon &= \log_2 \left(1 + \sum_{n \neq m} c_n c_m \right), \\ &= \log_2 \left(\sum_n c_n^2 + \sum_{n \neq m} c_n c_m \right), \\ &= \log_2 \left(\sum_n c_n \right)^2. \end{aligned} \quad (\text{A4})$$

For the c_n of Eq. (A1) corresponding to the EPH-embedded TMSV, $(\sum_n c_n)^2 = e^{4r} / \cosh 2r$, while for TMSV whose $c_n = \tanh^n r / \cosh r$, $(\sum_n c_n)^2 = e^{2r}$.

Appendix B

The fidelity of teleportation \mathcal{F} , as given in Eq. (18), involves the characteristic function of the entangled resource $\chi_{\text{EPR}}(-\alpha^*, -\alpha)$. $\chi_{\xi}(-\alpha^*, -\alpha)$ and $\chi_{\text{EPH}}(-\alpha^*, -\alpha)$ of Eq. (16), at the optimal value of phase $\phi = \pi$ in Eq. (17), take the simplified forms

$$\begin{aligned} \chi_{\xi}(-\alpha^*, -\alpha) &= e^{-\gamma|\alpha|^2}, \\ \chi_{\text{EPH}}(-\alpha^*, -\alpha) &= \frac{1 + 2 \tanh r |\alpha|^2 + \tanh^2 r (1 - |\alpha|^2)^2}{1 + \tanh^2 r} \\ &\quad \times e^{-\gamma|\alpha|^2}, \end{aligned} \quad (\text{A5})$$

respectively, where $\gamma = e^{-2r}$. The above expression for χ_{EPH} can be written as a differential of χ_{ξ} with respect to γ as:

$$\chi_{\text{EPH}}(-\alpha^*, -\alpha) = \hat{\Gamma} \chi_{\xi}(-\alpha^*, -\alpha), \quad (\text{A6})$$

where $\hat{\Gamma}$ is the differential operator given in Eq. (19). In calculating the fidelity of teleportation using EPH-embedded TMSV based on Eq. (18) (and also the Wigner function based on (Eq. 13)), since the integration is in-

dependent of the parameter γ , $\hat{\Gamma}$ can be pulled out of the integral. Hence, the final expression for the fidelity with EPH-embedded TMSV differs from that with TMSV only in having the differential operator $\hat{\Gamma}$ in front.